An Ionic Liquid Extraction That Preserves the Molecular Structure of Cutin Shown by Nuclear Magnetic Resonance[1][OPEN]

Carlos J.S. Moreira,[a,2] Artur Bento,[a,2] Joana Pais,[a] Johann Petit,[b] Rita Escórcio,[a] Vanessa G. Correia,[a] Ângela Pinheiro,[a] Łukasz P. Haliński,[c] Oleksandr O. Mykhaylyk,[d] Christophe Rothan,[b] and Cristina Silva Pereira[a,3,4]

[a]Instituto de Tecnologia Química e Biológica António Xavier, Universidade Nova de Lisboa, 2780–157 Oeiras, Portugal
[b]Institut National de la Recherche Agronomique, University of Bordeaux, UMR 1332 Biologie du Fruit et Pathologie, F–33140 Villenave d'Ornon, France
[c]Department of Environmental Analysis, Faculty of Chemistry, University of Gdańsk, 80–308 Gdańsk, Poland
[d]Soft Matter Analytical Laboratory, Dainton Building, Department of Chemistry, The University of Sheffield, Sheffield S3 7HF, United Kingdom

ORCID IDs: 0000-0002-7708-2505 (C.J.S.M.); 0000-0003-4097-1613 (A.B.); 0000-0002-8261-2099 (J.Pa.); 0000-0002-6746-1755 (J.Pe.); 0000-0003-3473-3686 (R.E.); 0000-0002-7357-7199 (V.G.C.); 0000-0002-4974-7143 (A.P.); 0000-0001-6970-7299 (Ł.P.H.); 0000-0003-4110-8328 (O.O.M.); 0000-0002-6831-2823 (C.R.); 0000-0002-6750-1593 (C.S.P.).

The biopolyester cutin is ubiquitous in land plants, building the polymeric matrix of the plant's outermost defensive barrier, the cuticle. Cutin influences many biological processes in planta; however, due to its complexity and highly branched nature, the native structure remains partially unresolved. Our aim was to define an original workflow for the purification and systematic characterization of the molecular structure of cutin. To purify cutin we tested the ionic liquids cholinium hexanoate and 1-butyl-3-methyl-imidazolium acetate. The ensuing polymeric materials are highly esterified, amorphous, and have a typical monomeric composition as demonstrated by solid-state NMR, complemented by spectroscopic, thermal, and x-ray scattering analyses. We performed a systematic study by solution-state NMR of cryogenically milled cutins extracted from tomatoes (*Solanum lycopersicum* 'Micro-Tom'; the wild type and the *GLYCEROL-3-PHOSPHATE ACYLTRANSFERASE* [*GPAT6*] and *CUTIN SYNTHASE* [*CUS1*] mutants). We resolved their molecular structures, relative distribution of ester aliphatics, free acid end-groups and free hydroxyl groups, differentiating between those derived from primary and secondary esters. Our data demonstrate the existence of free hydroxyl groups in cutin and provide insight into how the mutations affect the esterification arrangement of cutin. The usage of ionic liquids for studying plant polyesters has advantages over conventional approaches, since simple modifications can be applied to recover a biopolymer carrying distinct types/degrees of modifications (e.g. preservation of esters or cuticular polysaccharides), which in combination with the solution NMR methodologies developed here, constitutes essential tools to fingerprint the multifunctionality and the structure of cutin in planta.

Plant polyesters, namely cutin and suberin, are the third most abundant plant polymers after cellulose/hemicellulose and lignin. Naturally, due to their high abundance in nature, plant polyesters are considered as promising substitutes for petroleum-based plastics (Heredia-Guerrero et al., 2017). In particular, cutin makes up the polymeric matrix of the cuticle that builds the protective layer of the aerial parts of land plants; an evolutionary feature acquired during the colonization of terrestrial environments (Fich et al., 2016). The cuticle constituents (cutin and waxes) are deposited onto the polysaccharide layer of the walls of the epidermal cells (Segado et al., 2016). Cutin is, in general, a highly branched polymer, mainly composed of C16 and C18 fatty acids, containing mostly terminal (ω-hydroxyl) and midchain hydroxyl groups, linked through ester bonds. Other functional groups, such as aromatics, dicarboxylic acids, and glycerol, can also be found in cutin in low amounts (Mazurek et al., 2017).

Over the years, many authors have contributed to elucidate the roles played by cutin in diverse biological processes of plant development, growth, and response to biotic and/or abiotic stresses (Fich et al., 2016). However, current methods for the extraction and analysis of cutin polyesters have inherent limitations. The extraction of cutin from a plant source usually relies on time-consuming processes that include enzymatic digestion of polysaccharides followed by thorough organic solvent extraction of the soluble waxes present in the cuticle (Chatterjee et al., 2012). In addition, the chemical analyses of cutin used most frequently are based on total/partial hydrolysis of the polyesters and therefore disclose solely the monomeric constituents (Graça and Lamosa, 2010; Fernández et al., 2016), although sometimes solid-state spectroscopic based analyses of the polymer are used (Deshmukh et al., 2003; Fernández et al., 2016). The monomeric constituents can disclose a partial view of the basic composition

of the biopolymer (i.e. the hydrolyzable constituents), providing insights into its biosynthesis (Bakan and Marion, 2017), but they do not reveal the structural molecular organization, which remains largely unknown (Fich et al., 2016; Bakan and Marion, 2017). To advance our understanding of important cutin-related questions, such as interactions between cutin and the cell wall polymers or the role of cutin in defense against pathogens (Chatterjee et al., 2016), a better insight into the structure of cutin in its native state is required.

Ionic liquids, usually defined as salts in a liquid state below 100°C, may facilitate the processing of plant polymers due to their capacity to induce swelling/solubilization and/or catalyze the cleavage of specific intermolecular bonds (Rogers and Seddon, 2003). In particular, some imidazolium-based ionic liquids can efficiently disrupt the intermolecular hydrogen bonding between hydroxyl groups in cellulose (Li et al., 2018), whereas some cholinium alkanoates can catalyze selectively the hydrolysis of intermolecular acylglycerol esters (Garcia et al., 2010; Ferreira et al., 2012, 2014). The latter ionic liquid was used by us to extract suberin from cork (*Quercus suber*), a plant polyester sharing chemical similarities with cutin, by catalyzing a selective and mild hydrolysis of acylglycerol esters yet preserving most extant linear aliphatic esters (Ferreira et al., 2014; Correia et al., 2020).

Our aim was to establish a novel cutin extraction method that allows the study of near-native cutin architecture and properties and is applicable to a wide range of plant species and tissues. To meet these criteria, the method should be rapid and easy to process, and should greatly preserve the chemical structure of cutin. To this end, we first established an ionic liquid approach for the extraction of cutin, with the solubilization of cutin from tomato (*Solanum lycopersicum*) peels as a proof of concept. We demonstrated that the cholinium hexanoate process renders a material that is enriched in cutin, as shown by scanning electronic microscopy (SEM), ^{13}C magic angle spinning NMR (^{13}C MAS NMR), and differential scanning calorimetry (DSC) analyses of cutin structure. These analyses were complemented by gas chromatography-mass spectrometry (GC-MS) analyses of the hydrolyzable constituents. In addition, we established the molecular structure of cutins in solution (solubilized with the aid of cryogenic milling) through high-resolution one- and two-dimensional (2D) solution-state NMR analyses. Extension of our approach from a processing tomato cultivar to the miniature cv Micro-Tom, including two cutin biosynthesis and polymerization mutants, highlighted the consistency of our findings with published results but also revealed unknown features of cutin. We therefore believe that our methodological approach will support discovery in the field of cutin biogenesis and biosynthesis.

RESULTS

A Highly Esterified Cutin Was Purified Using Ionic Liquids That Mostly Mediate the Dissolution of Subcuticular Polysaccharides

Seeking to establish a method to extract cutin from tomato peels, we resorted to cholinium hexanoate and 1-butyl-3-methyl-imidazolium (BMIM) acetate. Cholinium hexanoate was chosen because of its ability to mediate the extraction of suberin from cork through mild and selective hydrolysis of acylglycerol ester bonds (Ferreira et al., 2014), and BMIM acetate was chosen for its proven ability to mediate the dissolution of cellulose (Li et al., 2018). First, we tested whether either ionic liquid (100°C without stirring) hydrolyzes glyceryl trioctanoate and octyl octanoate, which contain an acylglycerol ester bond and a linear aliphatic ester bond, respectively. Glyceryl trioctanoate was hydrolyzed in the presence of both ionic liquids, yet the efficiency of the reaction was higher when cholinium hexanoate was used (Fig. 1). Cholinium hexanoate did not catalyze the cleavage of octyl octanoate (Fig. 1A), whereas BMIM acetate did catalyze this reaction albeit inefficiently (Fig. 1B). As previously reported, cholinium hexanoate catalyzes specifically the hydrolysis of acylglycerol esters (Ferreira et al., 2014), although in this study the absence of agitation and the higher water content of the ionic liquid reduced the reaction efficiency.

We then tested the potential of these ionic liquids to isolate cutin from tomato peels after 2, 15, and 170 h compared to a conventional method (i.e. enzymatic removal of polysaccharides followed by organic solvent-mediated dewaxing). In the process of suberin extraction

[1]This work was supported by the European Research Council (grant no. ERC 2014–CoG–647928), the European Commission's Horizon 2020 research and innovation programme (project no. 713475–FLIPT–H2020–FETOPEN–2014-2015), the Fundação para a Ciência e Tecnologia (grant no. UID/Multi/04551/2019 [Research unit GREEN-it "Bioresources 4 Sustainability"] and project no. PTDC/AGR–TEC/1191/2014AAC), King's College London Medical Engineering Centre (Wellcome Trust EPSRC Centre of Excellence in Medical Engineering; capital equipment grant no. EP/M028437/1 to O.O.M.), and Aralab (PhD contract no. 06/PlantsLife/2017 to C.J.S.M.).

[2]These authors contributed equally to the article.

[3]Senior author.

[4]Author for contact: spereira@itqb.unl.pt.

The author responsible for distribution of materials integral to the findings presented in this article in accordance with the policy described in the Instructions for Authors (www.plantphysiol.org) is: Cristina Silva Pereira (spereira@itqb.unl.pt).

C.S.P. supervised the project and the interpretation of data and prepared the final version of the manuscript; J.Pe. and C.R. contributed to plant material preparation; C.J.S.M., A.B., and R.E. performed ionic liquid synthesis, cutin extraction, and cryogenic milling; A.B. and V.G.C. analyzed the NMR data; J.Pa., A.P., J.Pe., and L.H. analyzed the gas chromatography-mass spectrometry data; O.O.M. and A.B. analyzed the wide-angle x-ray scattering data); A.B. and C.J.S.M. analyzed the differential scanning calorimetry data; C.J.S.M. and A.B. prepared the initial draft of the manuscript; and all authors read and approved the final version of the article.

[OPEN]Articles can be viewed without a subscription.

www.plantphysiol.org/cgi/doi/10.1104/pp.20.01049

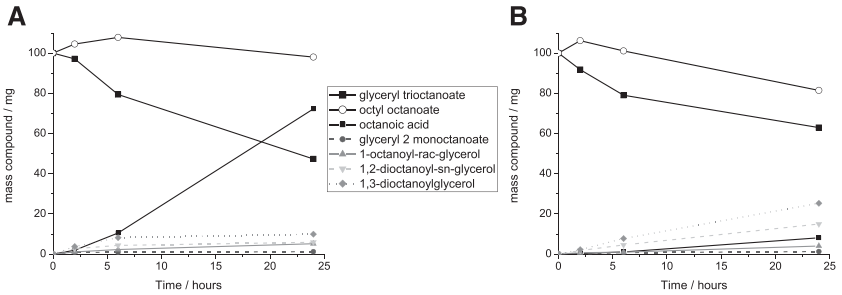

Figure 1. Quantitative analysis of the ionic liquid-mediated hydrolysis of ester bonds in model compounds. Compounds detected after the reaction of glyceryl trioctanoate and octyl octanoate with either cholinium hexanoate (A) or BMIM acetate (B) for 2, 6, and 24 h (the observed average SE values were negligible at <4%). All compounds were identified and quantified by GC-MS. At time zero, glyceryl trioctanoate and octyl octanoate were assumed to represent the only compounds present in the mixture.

from cork using cholinium hexanoate, suberin in the filtrate is recovered by precipitation in an excess of water (Ferreira et al., 2012). We preliminarily tested a 2-h reaction of tomato peel cutin in cholinium hexanoate and used attenuated total reflection-Fourier transform infrared spectroscopy (ATR-FTIR) to verify that the archetypal bands assigned to cutin, i.e. long-chain aliphatics (CH_2 and C=O), were detected in the insoluble fraction (not in the filtrate as observed for cork suberin) whereas the filtrate shows enrichment in bands usually assigned to polysaccharides (C-O-C; Supplemental Fig. S1). Accordingly, the insoluble fractions produced were characterized using SEM (Fig. 2) and ^{13}C MAS NMR (Fig. 3A). SEM imaging of the cutins extracted with either ionic liquid are virtually identical: a clean thick cutin-continuum showing the epidermal cell grooves (Fig. 2, A–F). In the reference cutin, i.e. obtained through the conventional enzymatic-based process, the cutin continuum apparently overlaps with other cellular components, and many intracellular spaces are not hollow (Fig. 2G).

In the ^{13}C MAS NMR spectrum of the reference cutin, the major structural classes assigned to cutin include the long methylene chains, $(CH_2)_n$, with major peaks at 26, 29, and 34 ppm; the oxygenated aliphatics, CH_2O (63 ppm) and CHO (73 ppm); and the carboxyl groups at 172 ppm, comprising the contribution of both esters and acids (Fig. 3A; Chatterjee et al., 2016). Only minor signals can be assigned to the aromatic region (105 and 130 ppm). The spectral signatures of the remaining cutins are very similar, regardless of the ionic liquid used and the extraction time, and are also similar to the reference cutin spectrum (Fig. 3; Table 1). The relative contributions of the signals assigned to aromatics for the cutins purified with either ionic liquid increased along the reaction time, possibly an artifact derived from phase corrections. The relative contributions of the oxygenated aliphatic region (57–92 ppm) are higher in ionic liquid-extracted cutins compared to the reference cutin (Fig. 3A). This region might also comprise resonances derived from polysaccharides (Chatterjee et al., 2016). Most subcuticular polysaccharides can be removed from cutin using acidic hydrolysis mediated by trifluoroacetic acid (TFA; Arrieta-Baez and Stark, 2006), although cellulose might not be totally removed (Hernández Velasco et al., 2017). In this study, the NMR spectra of cutins obtained using cholinium hexanoate (2-h reaction) before and after the acidic hydrolysis treatment are virtually identical (Table 1; Supplemental Fig. S2). The few observed alterations can be explained by the hydrolysis of esters during the acidic treatment (Arrieta-Baez and Stark, 2006). Based on these results, the oxygenated aliphatics region can be mostly assigned to cutin. Consequently, the biopolymer reticulation level can be reasonably estimated through the ratio of the signal's integral in the CHO region of the oxygenated aliphatics (67–92 ppm) to that of the entire aliphatic region (8–50 ppm) or that of the CH_2O region (57–67 ppm; Matas et al., 2011; Chatterjee et al., 2016). Based on the calculated reticulation ratios, cholinium hexanoate usage apparently rendered a biopolymer displaying higher reticulation compared to that attained with either BMIM acetate or the conventional approach (Fig. 3, B and C). At this stage, one cannot exclude that the presence of cellulose embedded in the biopolymer might increase the estimated reticulation levels. A similar trend was observed when estimating biopolymer esterification levels (Fig. 3D), which can be inferred through the ratio of the integral of the total oxygenated aliphatic region (CHO and CH_2O) with that of the entire aliphatic region (8–50 ppm; Matas et al., 2011). Esterification of the cholinium cation with cutin's free acids was reported previously to be mechanistically very unlikely (Ferreira et al., 2014).

In order to further elucidate whether the ionic liquid-based extractions can indeed render a material enriched in cutin, we resorted to DSC (Fig. 4A) and wide-angle x-ray scattering (WAXS; Fig. 4B) measurement of the cutins extracted with the ionic liquids (2- and 170-h reactions) together with the reference cutin. The DSC thermograms are depicted in Figure 4A. The cutins extracted using either ionic liquid for 2 h show higher enthalpy energies for melting the biopolymer and lower melting temperatures (ΔH = 129.6 J g^{-1} and T_m = 100.5°C versus ΔH = 97.5 J g^{-1} and T_m = 100.6°C, for cholinium hexanoate and BMIM acetate, respectively) compared to the reference cutin (ΔH = 70.5 J g^{-1} and T_m = 114.5°C). All thermograms show a relatively broad melting curve (Fig. 4A), which is typical for heterogeneous and amorphous materials (Benítez et al., 2018), and similar glass transition temperatures (~−20°C). The peaks for the cutins that originated from the 2-h ionic liquid reactions are less broad compared to the reference cutin, suggestive of increased homogeneity. This feature was lost when extensive reaction times were used, consistent with the estimated reduction in biopolymer reticulation and esterification (Fig. 3, B–D). The WAXS

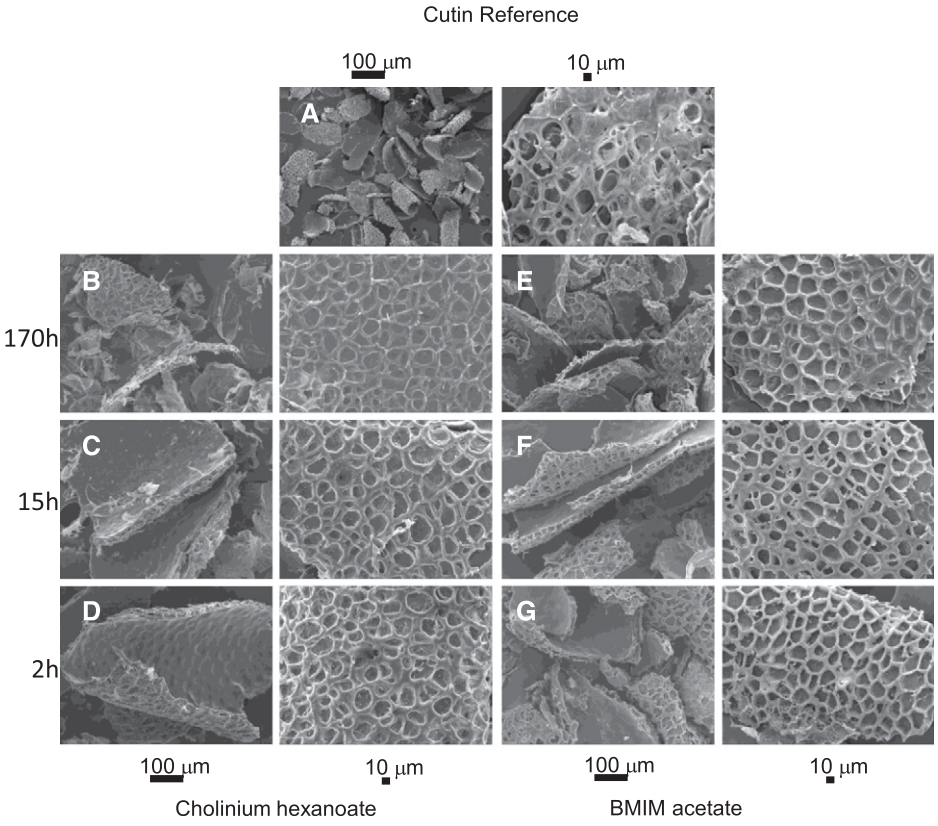

Figure 2. SEM analysis of cutin-enriched materials upon extraction. A, A representative cutin reference sample (i.e. obtained through the conventional enzymatic-based process) depicts many intracellular spaces that are not hollow. B to G, Imaging of cutin-enriched materials was obtained after treatment with cholinium hexanoate (B–D) or BMIM acetate (E–G) for 2, 15, and 170 h. All samples show a clean thick cutin-continuum comprising the epidermal cell grooves.

patterns of all cutin samples (Fig. 4B) are mainly represented by a broad diffuse peak with maximum intensity at around $q = 1.41$ Å^{-1}, which most likely corresponds to an amorphous structure commonly formed by organic polymeric materials with an interchain distance of ~4.5 Å. Considering the composition of cutin, this amorphous structure should be related to randomly packed acyl chains. In contrast to the reference cutin, the scattering patterns of cutins extracted by either ionic liquid show diffraction peaks indicating the presence of a crystalline component. The first diffraction peak at $q = 1.52$ Å^{-1} and the second at $q = 1.69$ Å^{-1}, noticeable

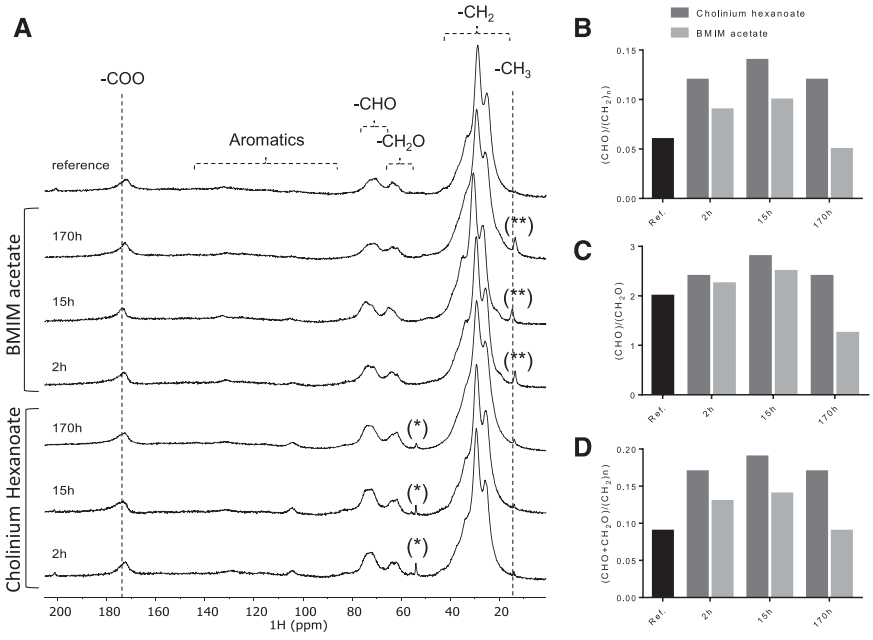

Figure 3. ^{13}C MAS NMR spectra obtained for the cutin-enriched materials upon extraction. Spectra of the reference cutin sample and cutin-enriched materials derived from reactions with cholinium hexanoate or BMIM acetate for 2, 15, and 170 h (A) and the corresponding calculated reticulation (B and C) and esterification (D) ratios. The regions assigned to the long methylene chains, oxygenated aliphatics, aromatics, and carboxyl groups are marked. The imidazolium-based cation contributes to the signal assigned to the CH_3 groups at 15 ppm (**), whereas the cholinium cation is seen in the signal at 54 ppm (*); both contaminants can be washed out.

Table 1. *Relative abundance of the contributions of the regions of aliphatics (10–50 ppm), oxygenated aliphatics (57–92 ppm), aromatics (92–165 ppm), and carboxyl groups (165–185 ppm) for each cutin ^{13}C MAS NMR spectrum*

Method	Cutin Major Structural Classes	Relative Abundance of the ^{13}C MAS NMR Assigned Regions				
		C=O	C=C	CHO	CH_2O	$(CH_2)_n$
		Carboxyls	Aromatics	Oxygenated Aliphatics		Aliphatics
				%		
Reference	—	5.1	1.7	5.1	2.6	85.5
Cholinium hexanoate	2 h	4.8	1.6	9.6	3.7	80.0
	2 h + TFA	3.9	3.1	10.2	4.7	78.1
	15 h	4.7	3.1	10.9	3.9	77.5
	170 h	4.7	3.1	9.1	3.9	65.0
BMIM acetate	2 h	5.6	4.0	7.2	3.2	80.0
	15 h	5.5	5.5	7.8	3.1	73.5
	170 h	5.6	6.5	4.0	3.2	80.6

for cutin extracted by cholinium hexanoate for 170 h (Fig. 4A, blue curve), can be assigned to an orthorhombic crystal structure (space group Pnma; Miller indexes 110 and 200, respectively) commonly formed by compounds comprised of alkane-like chains such as triacylglycerols (b′ phase; Mykhaylyk et al., 2007) or polyethylene (Bunn, 1944; Southern et al., 1972). This suggests that the extraction of cutin by the ionic liquids enriches this material with a crystalline component where some acyl chains tend to form crystals. A low level of branching of acyl chains in cutin may be favorable for the formation of an orthorhombic unit cell, which is thermodynamically more stable than the rotator phase formed by distorted alkane chains packed in a hexagonal array (Small, 1984). This observation is consistent with the DSC measurements (Fig. 4A) indicating that the cutin extracted by cholinium hexanoate for 170 h, containing the highest fraction of the acyl crystalline component, has the highest peak melting point. The third diffraction peak, at $q = 2.46$ Å^{-1}, observed for cutin extracted by cholinium hexanoate (Fig. 4B, purple and blue curves), cannot be related to the acyl chain crystalline structure. Its position is significantly shifted from a possible 020 peak at $q = 2.55$ Å^{-1} generated by the orthorhombic structure (Fig. 4B). The third peak is likely to be associated with a crystalline cellulose and can be assigned to 004 reflection of monoclinic cellulose I_β (space group $P12_11$; Rongpipi et al., 2019). It must be noted that the most intense 200 diffraction peak of the cellulose I_β expected at $q = 1.63$ Å^{-1} is not visible because of an overlap with the intense broad peak corresponding to the amorphous structure. Crystalline cellulose usually coexists with amorphous cellulose (Rongpipi et al., 2019). However, it would be difficult, if possible at all, to identify the amorphous cellulose component, with its expected peak maximum intensity at $q = 1.52$ Å^{-1}, from the broad diffuse peak observed

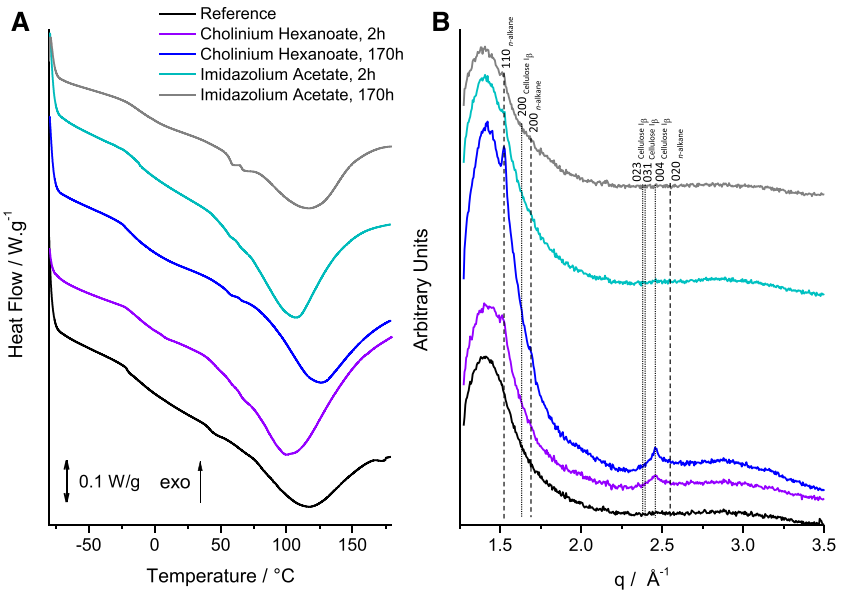

Figure 4. Analysis of the crystallinity properties of the cutin-enriched materials upon extraction. DSC thermograms (A) and WAXS patterns (B) collected for a reference enzymatically extracted cutin material (black curve) and cutin materials extracted from tomato peels using ionic liquids for various durations of treatment: cholinium hexanoate for 2 and 170 h (purple and blue curves, respectively) and imidazolium acetate for 2 and 170 h (gray and cyan curves, respectively). The vertical straight lines in WAXS patterns indicate the positions of diffraction peaks of cellulose (dotted lines) and crystallized n-alkane chains (dashed lines). Miller indexes assigned to the lines correspond to cellulose I_β (monoclinic space group $P12_11$) and n-alkane chain packing (orthorhombic space group Pnma).

by WAXS. Neither enzymatically extracted cutin (reference cutin) nor cutin extracted by BMIM acetate reveal the presence of crystalline cellulose in their scattering patterns (Fig. 4B, black, cyan, and gray curves), indicating that both extraction methods led to its successful removal. This observation, together with the higher relative contribution of the oxygenated aliphatics region for cutin extracted with BMIM acetate compared with the reference cutin (Table 1), suggests that some oxygenated aliphatics are lost during the enzymatic treatment.

Finally, the relative abundances of hydrolyzable cutin constituents were determined by GC-MS to disclose how ionic liquid extraction methods influence the composition of the biopolymer compared to the reference method (Table 2; Supplemental Fig. S3; Supplemental Table S1). The reference cutin comprises ~13% of non-hydrolyzable constituents, whereas cutin constituents attained using an ionic liquid display substantially higher recalcitrance (~20% to 30%), consistent with their estimated higher reticulation (Fig. 3, B and C). In general, the monomeric compositions of the ionic liquid-extracted cutins are similar to that of the cutin reference (and also to the starting material; Table 2). Both the abundance and the diversity of fatty acids decreased as the reaction time in the ionic liquid increased (Table 2). This was more pronounced when BMIM acetate was used for 170 h, which rendered a cutin almost devoid of fatty acids and also containing nearly 2-fold less dicarboxylic acids. The fatty acids carry a methyl end-group that is esterified to the biopolymer through a single bond.

A Snapshot of the Molecular Structure of Cutin Purified by Cholinium Hexanoate Reveals Extant Free Hydroxyls and Free Acids

Our data made evident the potential of using short-time reactions with either ionic liquid to recover from tomato peels a cutin continuum displaying esterification/reticulation levels and composition near that found in planta. In addition, cholinium hexanoate presents several advantages compared to BMIM acetate. It cleaves fewer ester bonds, rendering a more esterified biopolymer (Fig. 3D), and unlike BMIM acetate, it is also biocompatible and biodegradable (Petkovic et al., 2010).

Recently, we used solution-state NMR to resolve the molecular structure of in situ suberin upon its solubilization in heated dimethylsulfoxide (DMSO) directly from cork after 4 h of cryogenic milling (Correia et al., 2020). This inspired us to apply cryogenic milling for the solubilization of a cutin extracted with cholinium hexanoate after 2 h. Solving cutin's molecular structure would allow us to look "inside" its backbone, specifically at its esterification arrangement. The GC-MS analyses disclosed only the component hydrolyzable constituents (Table 2) and the solid-state analyses—^{13}C MAS NMR, DSC, and WAXS (Figs. 3 and 4)—revealed only the bulky chemical functionalities and properties of the purified cutin materials. Only after 10 h of cryogenic milling was the cutin solubilized in DMSO, reflecting cutin's much lower solubility compared to suberin. We analyzed the impact of the cryogenic milling process, especially the occurrence of oxidation reactions inside the grinding jar due to possible condensation of oxygen at low temperatures. Elemental analysis of cutin before and after the cryogenic milling process revealed that the relative percentages of the tested elements, including oxygen (Supplemental Table S2), were unaltered after the treatment. Therefore, despite the solubility drawback, a solution-state ^{1}H NMR could be acquired with good resolution, showing the presence of many overlapping signals (Fig. 5A), an archetypal feature observed in other complex multifunctional polymers (Lyerla, 1980). The relative abundances of aliphatics, CH/CH_2-X oxygenated aliphatics, and aromatics were estimated through integration of the ^{1}H spectrum as 70%, 27%, and 3%, respectively. The assignment of ^{1}H chemical shifts for the constituent monomers was then achieved through a combination of ^{1}H-^{1}H correlation spectroscopy (COSY) and ^{1}H-^{13}C correlations, namely heteronuclear single-quantum correlation spectroscopy (HSQC) and heteronuclear multiple-bond correlation spectroscopy (HMBC; Supplemental Figs. S4–S6; Supplemental Table S3). Previous NMR-based data for tomato cutin were attained through solution-state NMR analyses of oligomeric structures obtained by methanolysis of tomato peels (Graça and Lamosa, 2010) and high-resolution MAS NMR analyses of tomato cutin swollen in DMSO (Deshmukh et al., 2003). These studies provided important baseline information for the assignment of the spectrum of cutin extracted with cholinium hexanoate for 2 h (Supplemental Table S3).

The full range of the HSQC spectrum of cutin is depicted in Figure 5B, which highlights the regions corresponding to aliphatics and CH/CH_2-X aliphatics as well as aromatics. A detailed analysis of the HSQC spectrum of the two aliphatic regions with the assignment of CH_2 and CH_3 groups from the aliphatic chains, the ester bonds, and the free midchain hydroxyl groups is shown in Figure 5, C and D. Only secondary free hydroxyl groups were visible in the HSQC spectrum (CHOH midchain), consistent with their presence in cutin as suggested previously (Philippe et al., 2016). This observation is in agreement with the demonstration that cholinium hexanoate does not cleave primary ester bonds (Fig. 1). Here, we assigned the β-(C=O) esters to a ^{1}H shift of 1.49 ppm and a ^{13}C shift of 24 ppm, but we could not detect the signal of β-(C=O) acids, even though they have been assigned before in tomato cutin using high-resolution MAS NMR (Deshmukh et al., 2003). Deshmukh et al. (2003) assigned the signals of aliphatic esters, primary and secondary alcohols, free acids, and α-branched carboxylic acids, yet the last two assignments could not be confirmed by HMBC. In this study, the signals of the β-(C=O) acids may overlap with that of the esters, and differentiating these signals from the small chemical shift differences observed in the acquired HSQC data is virtually impossible.

Table 2. *GC-MS quantitative analysis of the hydrolyzable constituents identified in cutin samples purified using either cholinium hexanoate or BMIM acetate in 2-, 15-, or 170-h reactions*

The reference cutin and the feedstock (i.e. untreated peels) were also analyzed for comparison. Results are given as wt % (n = 3). The identification yields (wt %) and the mass of the nonhydrolyzable fraction (recalcitrance [%]) are indicated.

Compound Name	Compound Abundances							
	Untreated Feedstock	Reference Cutin	Cholinium Hexanoate			BMIM Acetate		
			2 h	15 h	170 h	2 h	15 h	170 h
					wt %			
Fatty acids	2.60 ± 0.13	1.52 ± 0.24	1.27 ± 0.15	0.88 ± 0.13	0.67 ± 0.09	1.96 ± 0.2	0.74 ± 0.1	0.10 ± 0.06
Hexadecanoic acid	1.25 ± 0.04	0.74 ± 0.05	0.64 ± 0.04	0.41 ± 0.11	0.33 ± 0.03	0.63 ± 0.05	0.42 ± 0.03	0.10 ± 0.06
Octadeca-9,12-dienoic acid	0.43 ± 0.15	0.23 ± 0.05	0.20 ± 0.03	0.11 ± 0.01	–	0.74 ± 0.12	–	–
Octadec-9-enoic acid	–	0.24 ± 0.06	0.11 ± 0.02	0.09 ± 0.04	–	0.18 ± 0.03	–	–
Octadecanoic acid	0.91 ± 0.12	0.31 ± 0.10	0.09 ± 0.00	0.13 ± 0.05	0.12 ± 0.02	0.18 ± 0.04	0.13 ± 0.06	–
4-Oxocyclohexane-1-carboxylic acid	–	–	0.23 ± 0.08	0.14 ± 0.12	0.22 ± 0.06	0.23 ± 0.00	0.19 ± 0.02	–
Dicarboxylic acids	10.89 ± 1.08	18.38 ± 0.44	18.64 ± 0.49	19.2 ± 2.16	18.64 ± 0.58	18.45 ± 1.19	19.3 ± 0.21	9.99 ± 2.05
Nonanedioic acid[a]	–	0.43 ± 0.02	0.26 ± 0.02	0.26 ± 0.15	0.36 ± 0.01	0.27 ± 0.02	0.22 ± 0.04	–
Hexadecanedioic acid	0.56 ± 0.02	1.51 ± 0.07	1.30 ± 0.07	1.52 ± 0.10	1.22 ± 0.08	1.47 ± 0.07	1.42 ± 0.15	0.46 ± 0.07
8/9-Hydroxyhexadecanedioic acid[b]	10.33 ± 1.06	16.43 ± 0.38	17.08 ± 0.55	17.43 ± 2.01	17.06 ± 0.50	16.7 ± 1.14	17.66 ± 0.20	9.53 ± 0.23
ω-Hydroxy acids	11.13 ± 0.35	15.04 ± 0.31	18.42 ± 0.63	17.42 ± 2.22	17.69 ± 1.28	18.95 ± 0.4	18.49 ± 1.06	22.90 ± 1.68
16-Hydroxyhexadecanoic acid	5.38 ± 0.16	8.17 ± 0.21	8.20 ± 0.12	8.50 ± 0.65	8.32 ± 0.21	8.35 ± 0.23	8.48 ± 0.39	15.71 ± 0.68
16-Hydroxy-10-oxohexadecanoic acid	3.02 ± 0.28	2.29 ± 0.14	6.39 ± 0.52	6.21 ± 0.97	6.28 ± 0.61	6.81 ± 0.05	6.62 ± 0.39	1.80 ± 0.12
9, 10-Epoxy-18-hydroxyoctadecanoic acid	1.14 ± 0.24	1.93 ± 0.09	1.73 ± 0.07	1.63 ± 0.38	1.27 ± 0.32	1.67 ± 0.13	1.60 ± 0.14	2.38 ± 0.53
9, 10-Epoxy-18-hydroxyoctadecenoic acid	1.60 ± 0.15	2.65 ± 0.20	2.10 ± 0.25	1.62 ± 0.18	1.82 ± 0.55	2.11 ± 0.09	1.79 ± 0.18	3.01 ± 0.59
Polyhydroxy acids	55.05 ± 2.01	65.06 ± 0.65	61.67 ± 0.28	62.49 ± 4.06	63.01 ± 1.92	60.64 ± 1.69	61.47 ± 1.28	67.01 ± 1.44
10,16-Dihydroxyhexadecanoic acid[c]	53.22 ± 2.23	63.24 ± 0.98	58.83 ± 0.42	59.68 ± 5.03	61.20 ± 2.16	58.12 ± 1.89	58.97 ± 1.55	63.12 ± 2.42
9,10,18-Trihydroxyoctadecanoic acid	1.00 ± 0.11	0.94 ± 0.06	1.11 ± 0.32	1.19 ± 0.67	0.53 ± 0.00	0.85 ± 0.11	0.90 ± 0.13	1.51 ± 0.45
9,10,18-Trihydroxyoctadec-12-enoic acid	0.84 ± 0.39	0.89 ± 0.36	1.73 ± 0.07	1.63 ± 0.38	1.27 ± 0.32	1.67 ± 0.13	1.60 ± 0.14	2.38 ± 0.53
Sterols[d]	20.33 ± 1.07	–	–	–	–	–	–	–
Identification yield (%)	56.38 ± 2.46	50.7 ± 2.38	58.1 ± 0.88	59.34 ± 6.63	56.39 ± 1.20	58.02 ± 2.45	60.35 ± 3.46	82.15 ± 0.20
Recalcitrance (%)	22.14 ± 2.98	13.32 ± 1.39	28.3 ± 4.98	27.47 ± 0.58	33.07 ± 0.56	19.75 ± 0.36	20.21 ± 1.06	18.15 ± 2.48

[a]This compound was overestimated or overlapped with an unknown compound. [b]This compound was associated with the possible presence of unspecific isomers. [c]The major species of this compound was 10,16-diOH and minor species were 9,16- and 8,16-diOH. [d]Triterpenoids and sterols identified were β-amyrin (5.69 ± 0.44), α-amyrin (4.44 ± 0.20), δ-amyrin (7.53 ± 1.48), and stigmasterol (2.68 ± 0.49).

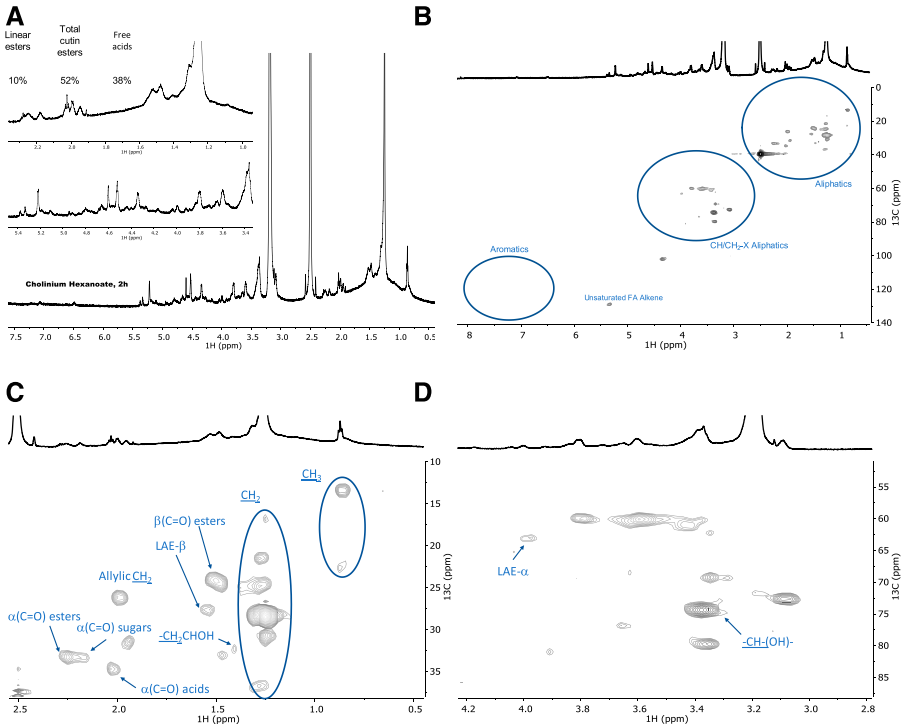

Figure 5. Wide-ranging NMR spectral characterization of cutin materials isolated with cholinium hexanoate (2 h). Shown are ^{1}H NMR spectra with inserts focusing on the aliphatic and oxygenated aliphatic regions (A) and the full HSQC spectrum (B) as well as regions corresponding to aliphatics (C) and CH/CH_2-X aliphatics (D) of the purified cutin. Some assignments (unlabeled) are uncertain or unidentified.

The α-(C=O) signal displays two ^{1}H signals with a ^{13}C shift of 33 ppm, namely at 2.25 and 2.19 ppm, which can be assigned to esters and acids, respectively. The α-(C=O) signal with a ^{1}H shift of 2.17 ppm was previously assigned to xylan esters (Zhang et al., 2016). Based on the detection of vestigial amounts of microcrystalline cellulose in the cutin extracted with cholinium hexanoate for 2 h (Fig. 4B), this signal may be associated with the presence of cellulose esters. Analysis of the cutin extracted with BMIM acetate (also cryogenically milled), which is apparently devoid of microcrystalline cellulose (Fig. 4B), showed that the α-(C=O) signal displays a ^{13}C shift of 33 ppm and only a ^{1}H shift of 2.26 ppm (Supplemental Fig. S7). Finally, to precisely assign the free acids in the cutin extracted with cholinium hexanoate for 2 h, we acquired the HMBC spectrum that confirmed their signal at a ^{13}C shift of 35 ppm and a ^{1}H shift of 2.02 ppm (Supplemental Fig. S6), consistent with the previously observed assignment in cork suberin, where the signal of the acids is at a ^{13}C shift of 36 ppm and a ^{1}H shift of 2.03 ppm and that of the esters displays a ^{13}C shift of 34 ppm and a ^{1}H broad shift from 2.33 to 2.27 ppm (Correia et al., 2020).

Based on the assignments defined above, we calculated the relative abundance of free acids, total esters (comprising primary and secondary aliphatic esters yet excluding sugar esters), and linear esters as 38%, 52%, and 10%, respectively, through integration of the signals in the ^{1}H NMR (Fig. 5A). No acylglycerol bonds were detected in the HSQC analyses of cutin (Fig. 5B), consistent with the very low abundance of glycerol in tomato cutin (Fich et al., 2016). We hypothesize that the free acids detected in the cutin spectra might mostly account for their natural occurrence, though one cannot exclude, at this stage, that some aliphatic esters might have undergone cleavage in the presence of cholinium hexanoate.

Ionic Liquid Extraction Followed by Solution NMR As a Tool to Scrutinize the Impact of Specific Mutations in the Molecular Structure of Cutin from cv Micro-Tom Tomatoes

Solving the molecular structure in solution of a near-native cutin isolated from a processing tomato cultivar challenged us to test the suitability of the established cholinium hexanoate extraction for 2 h for purification and systematic characterization of cutins isolated from the tomato miniature 'Micro-Tom', which is particularly well suited for laboratory studies (Just et al., 2013; Garcia et al., 2016). To introduce known diversity in cutin composition and structure, we further used both the wild type and mutants of *gpat6* and *cus1*, respectively (Petit et al., 2016, 2017; Philippe et al., 2016), which show phenotypes with altered cutin composition and altered degrees of intrachain branching. In particular, in the *gpat6* mutant (formerly named the cutin-deficient mutant, *cud1*; Philippe et al., 2016), synthesis of the major cutin precursor is hampered so that a thinner cuticle enriched in fatty acids is produced with overall decreased levels of cutin (Petit et al., 2016). In contrast, in the *cus1* tomato mutants, cutin polymerization is impaired (Girard et al., 2012; Yeats et al., 2012) and the esterification of secondary OH groups of the dihydroxy acids is significantly reduced (Philippe et al., 2016). To minimize any possible effect of environmental

conditions on the expression of the fruit cuticle phenotype, the *gpat6* and *cus1* mutants were grown side by side with wild-type plants. The relative abundance of the hydrolyzable constituents in the cv Micro-Tom cutins purified with cholinium hexanoate is depicted in Table 3. In general, the observed diversity/abundance of hydrolyzable constituents is similar to that previously reported (Petit et al., 2016; Philippe et al., 2016), though there are some variations, possibly due to disparities in tomato growth conditions in the greenhouse (season, light, temperature, and hygrometry). In addition, the cutins that originated from the mutants show an increase in the relative abundance of nonhydrolyzable constituents compared to the wild type (~10% increase), and their identification yields decreased nearly 20% due to higher diversity of unidentified monomers (Table 3). Cutin from both mutants displays a higher relative abundance of fatty acids and dicarboxylic acids (nearly 10- and 2-fold, respectively) and lower relative abundance of ω-hydroxyacids (five to three times) compared to wild-type cutin.

To confirm that free acids naturally occur in cutin (hence differentiating these from free acid groups formed during the ionic liquid extraction), we compared the spectra of cutin from the wild-type cultivar obtained through the ionic liquid process followed by cryogenic milling with that of the cuticle solubilized solely via cryogenic milling (Fig. 6; Supplemental Figs. S8–S12). The obtained ^{1}H NMR (Fig. 6, A and B) and HSQC spectra (Fig. 6, C–F) are very similar, although the presence of noncutin constituents in the cuticle contributes to the appearance of many signals that have yet to be assigned, e.g. in the CH_3 region (Fig. 6D). Importantly, the signals previously assigned to free acids α-(C=O) acids are visible in both samples (Fig. 6, C and D), as confirmed in the corresponding HMBC spectra (Supplemental Fig. S10). Accordingly, the free acids detected in the ionic liquid-purified cutins (Figs. 5, A–C, and 6, A and B) reflect their natural presence. The signal attributed to the terminal hydroxyls was only detected in the spectrum of the ionic liquid-extracted cv Micro-Tom cutin (Fig. 6E). This observation suggests that the cholinium hexanoate treatment cleaved some primary esters in the cv Micro-Tom cutin, contrary to observations for cutin derived from the peels of processing tomatoes (Fig. 5D). One possibility is that the cleavage of primary esters is greatly influenced by the native arrangement of the polymer.

The impact of the mutations is seen by the relative abundances of aliphatics, CH/CH_2-X oxygenated aliphatics, and aromatics in the ^{1}H-spectra, which were estimated as 71%, 29%, and 0% for the wild type

Table 3. *GC-MS quantitative analysis of the hydrolyzable constituents in cutin samples purified using cholinium hexanoate (2 h reaction) from wild-type and* cus1 *and* gpat6 *mutant 'Micro-Tom' tomato plants*

Results are given as % wt (n = 3). The identification yields (wt %) and the mass of the non-hydrolysable fraction (recalcitrance, %) are indicated below.

Compound Name	Compound Abundances		
	wt	*cus1*	*gpat6*
		wt %	
Fatty acids	0.50 ± 0.04	6.06 ± 0.81	5.60 ± 0.88
Hexadecanoic acid	0.27 ± 0.02	2.09 ± 0.26	1.59 ± 0.23
9,12-octadecadienoic	–	3.00 ± 0.59	2.22 ± 0.42
9-octadecenoic acid	0.24 ± 0.06	–	1.20 ± 0.16
Octadecanoic acid	–	0.96 ± 0.12	0.59 ± 0.11
Dicarboxylic acids	4.68 ± 0.32	7.23 ± 0.55	7.92 ± 0.5
Nonanedioic acid[a]	–	1.75 ± 0.37	0.88 ± 0.05
Hexadecandioic acid	0.60 ± 0.10	–	1.95 ± 0.23
8/9-hydroxyhexadecanedioic acid[b]	4.08 ± 0.23	5.48 ± 0.24	5.09 ± 0.25
ω-Hydroxy acids	5.47 ± 0.30	1.19 ± 0.02	1.56 ± 0.08
16-Hydroxyhexadecanoic acid	3.97 ± 0.23	1.19 ± 0.02	1.12 ± 0.09
16-Hydroxy-10-oxohexadecanoic acid	0.71 ± 0.04	–	0.44 ± 0.02
9, 10-Epoxy-18-hydroxyoctadecanoic acid	0.25 ± 0.05	–	–
9, 10-Epoxy-18-hydroxyoctadecenoic acid	0.54 ± 0.02	–	–
Polyhydroxy acids	89.35 ± 0.63	85.33 ± 1.32	84.86 ± 1.46
Dihydroxyhexadecanoic acid[c]	87.91 ± 0.48	83.87 ± 1.52	77.71 ± 2.50
9,10,18-Trihydroxyoctadecanoic acid	0.62 ± 0.06	0.91 ± 0.18	3.84 ± 0.76
9,10,18-Trihydroxyoctadec-12-enoic acid	0.82 ± 0.09	0.54 ± 0.04	3.31 ± 0.49
Sterols[d]	–	0.19 ± 0.04	–
Identification yield (%)	57.99 ± 1.26	37.49 ± 0.74	36.05 ± 1.75
Recalcitrance (%)	32.6 ± 3.68	44.26 ± 2.96	41.28 ± 0.97

[a]This compound was overestimated or overlapped with an unknown compound. [b]This compound was associated with the possible presence of unspecific isomers. [c]The major species of this compound was 10,16-diOH and minor species were 9,16- and 8,16-diOH. [d]The identified sterol was stigmasterol.

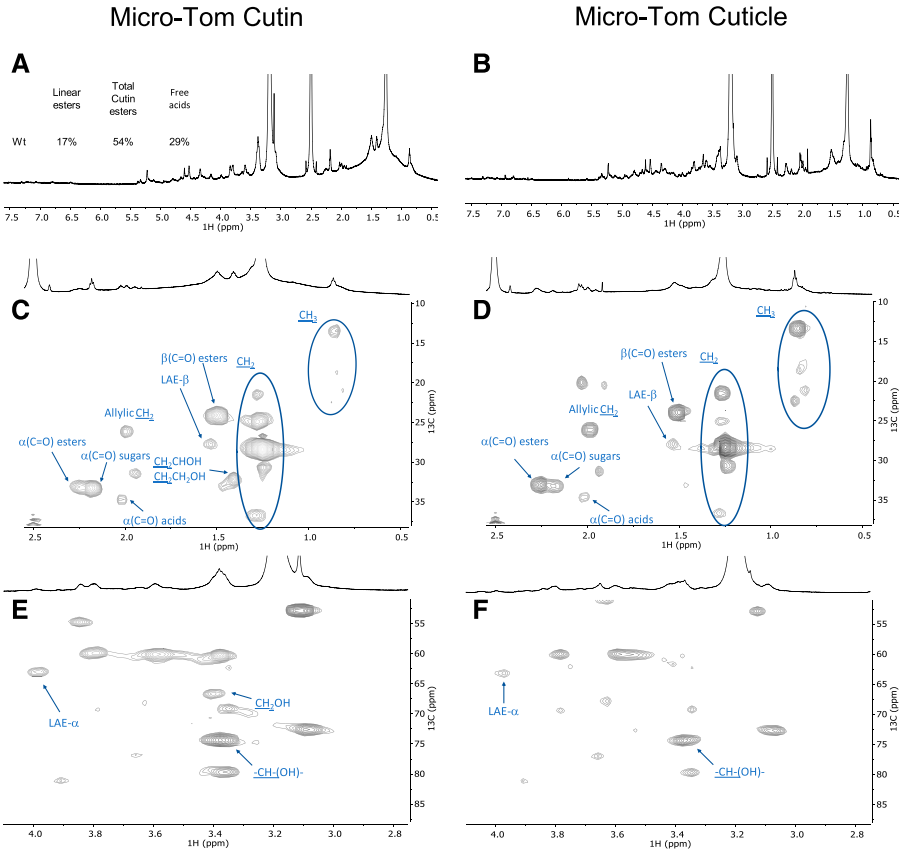

Figure 6. Wide-ranging NMR spectral characterization of Micro-Tom cutin isolated with cholinium hexanoate (2 h) and Micro-Tom untreated cuticle. The ^{1}H NMR spectra of cutin (A) and cuticle (B) samples, indicate the relative abundance (percent) of linear aliphatic esters (LAE-α), total esters [α(C=O) esters], and free acids [α(C=O) acids]; HSQC regions correspond to cutin (C) and cuticle (D) aliphatics and CH (E) and CH_2-X aliphatics (F). Some assignments (unlabeled) are uncertain or unidentified.

(Fig. 6A); 46%, 50%, and 4% for the *gpat6* mutant (Fig. 7A); and 39%, 59%, and 2% for the *cus1* mutant (Fig. 7B), respectively. In contrast to the wild type, the signal assigned to free acids could not be detected in either mutant (Fig. 7). To confirm this observation, we compared the spectrum of cutin from the *cus1* mutant purified by the ionic liquid followed by cryogenic milling with that of the *cus1* cuticle solubilized solely via cryogenic milling (Supplemental Fig. S13). The obtained HSQC spectra confirmed the absence of free acids in this mutant, further validating that the observed absence of this chemical group in the *cus1* and *gpat6* cutins is a consequence of the mutations and not of the sample processing (for further details, see Supplemental Figs. S8–S19).

Based on the ^{1}H-spectral information, we also estimated the relative abundance of aliphatic esters (total percent) and primary aliphatic esters in the cutin of the mutants (Fig. 7). Accordingly, the ratio of total esters versus linear esters is comparable in the wild type and the *gpat6* mutant but substantially lower in the *cus1* mutant. In other words, compared to the wild type, the *gpat6* mutant shows similar amounts of linear esters and secondary esters, in contrast to the *cus1* mutant, which shows a >2-fold increase in linear esters but also the lowest esterification level (i.e. amount of secondary esters; Fig. 7, A and B).

The magnification of the HSQC regions corresponding to aliphatics and CH/CH2-X aliphatics for the cutins of the mutants is also shown (Fig. 7, C–F; Supplemental Fig. S20). For both mutants, the signals assigned to terminal hydroxyls are visible (Fig. 7, E and F), similar to that observed in the wild-type cutin (Fig. 6E). The detected CH_3 groups are apparently enriched in both mutants compared to the wild type, consistent with the observed increase in relative abundance of hydrolyzable fatty acids for the mutants (Table 3) and with observations reported previously (Petit et al., 2016; Philippe et al., 2016). No acylglycerol was visible in the HSQC spectra of the cutin from the mutants, possibly because their abundance is below the detection limits of the analytical technique. The mutants show more nonassigned signals compared to wild-type cutin, consistent with the observed lower identification yields in the GC-MS data (Table 3). This might reflect also an altered diversity of cuticular polysaccharides in the mutants, a hypothesis that deserves further analysis in the near future and is sustained by recently published results for the *cus1* mutant (Philippe et al., 2020).

DISCUSSION

Considerable advances have been made in recent years on cuticle formation and properties (Nawrath et al., 2013). However, while the successive steps of cutin biosynthesis, transport of precursors, and polymerization in the

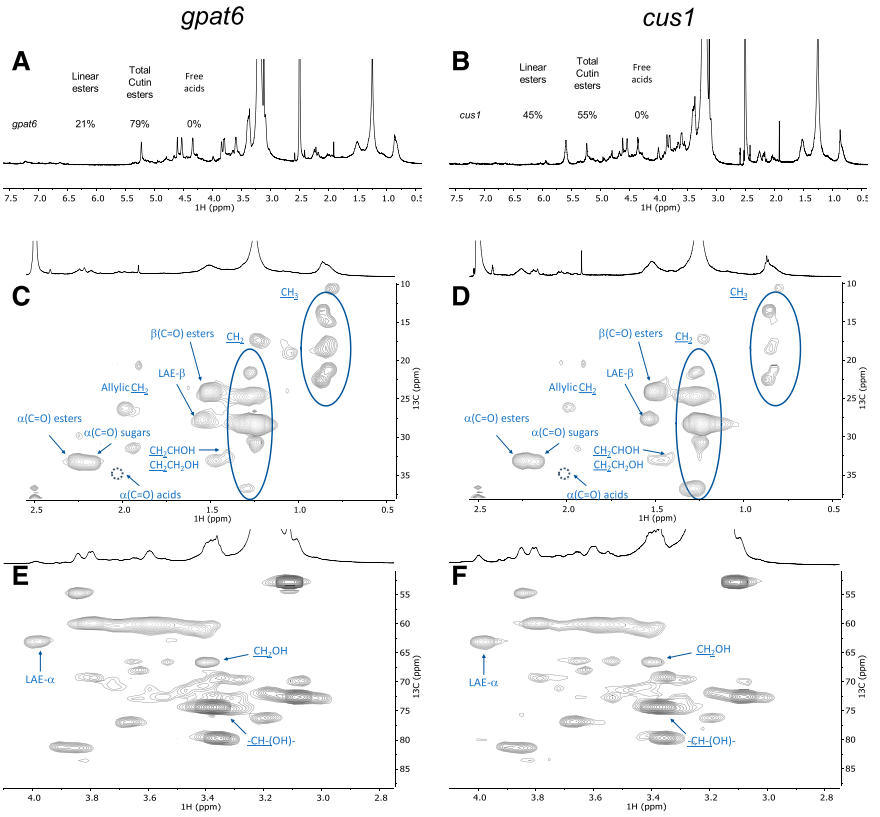

Figure 7. Wide-ranging NMR spectral characterization of cv Micro-Tom cutins isolated with cholinium hexanoate (2 h) from the *cus1* and *gpat6* mutants. A and B, ^{1}H NMR spectra of both samples (*gpat6* [A] and *cus1* [B]), showing the relative abundance (percent) of linear aliphatic esters (LAE-α), total esters [α(C=O) esters], and free acids [α(C=O) acids]. C to F, HSQC regions corresponding to aliphatics (C and D) and CH/CH_2-X aliphatics (E and F). Some assignments (unlabeled) are uncertain or unidentified. The absence of the signal assigned to α(C=O) acids is marked by a dashed circle. For simplicity, the wide-ranging NMR spectrum of the untreated cuticle from the *cus1* mutant is not shown (see Supplemental Fig. S13 for details).

epidermal cell walls begin to be well untangled (Fich et al., 2016), the questions of the fine structure of the cutin layer and its association with polysaccharides are still largely unresolved (Philippe et al., 2020). An example of the intricate relationships between cutin, cell walls, and resistance to pathogens is provided by the tomato *gpat6* mutant analyzed herein, in which the mutation has a profound impact not only on cutin synthesis (Petit et al., 2016) but also on cell walls (Philippe et al., 2020) and resistance to filamentous pathogens (Fawke et al., 2019). Insights into the structure and composition of native *gpat6* cutin would help considerably in deciphering the underlying mechanisms. More generally, the simple and rapid cutin extraction method described here, which preserves cutin in a near-native state, will help our understanding of the role of cuticle in plant evolution and diversity (Yeats et al., 2012, 2014), plant development (Ingram and Nawrath, 2017), mechanical properties of the organ surface (España et al., 2014; Mazurek et al., 2017), resistance to pathogens (Chassot et al., 2007), and fruit quality (Petit et al., 2017).

Advantages of Ionic Liquid Extraction with Respect to Conventional Cutin Extraction Methods

Our ionic liquid cutin extraction method performed on tomato peels, similar to the enzyme treatment method (Chatterjee et al., 2012), demonstrates that subcuticular polysaccharides (which were found in the filtrate) are removed, but does so in a considerably shorter time (i.e. 2 h instead of days, and even weeks). Also, the ionic liquid extraction does not require any specific dewaxing step. When extracted with either ionic liquid, a cutin continuum is isolated, strengthening the suggestion that the ionic liquid does not substantially impact the cutin polyester. This contrasts with our previously reported results for suberin extraction from cork using cholinium hexanoate, where nanoparticles of the biopolymer are isolated (Correia et al., 2020) because the ionic liquid catalyzes the mild cleavage of acylglycerol ester bonds (Ferreira et al., 2014), which are not representative in tomato cutin.

Cholinium Hexanoate Extraction Preserves Features of Cuticular Polysaccharides

In this study, purification of the cutin continuum by ionic liquids is essentially due to the dissolution of the subcuticular polysaccharides and, to a minor extent, ester cleavage. Under the conditions of the extraction used here, both ionic liquids cleaved ester bonds very inefficiently; however, cholinium hexanoate apparently cleaves only the acylglycerol bonds, whereas BMIM acetate can also cleave linear ester bonds. Hence, the cholinium hexanoate presents the advantages of biocompatibility and milder cleavage of the polymer backbone. The most remarkable difference between the two is that only the cholinium hexanoate could preserve features of cuticular polysaccharides, which

were specifically associated with the presence of microcrystalline cellulose. Cellulose with high levels of crystallinity was recently identified within the group of cutin-embedded polysaccharides (Philippe et al., 2020), consistent with the ability of the ionic liquid process to speedily recover cutin with a near-native structure. This opens unexpected possibilities for exploiting both ionic liquids, alone or in combination, to study the association and function of cuticular polysaccharides.

Cholinium Hexanoate Extraction Confirms the Presence of Free Hydroxyls in Native Cutin and Highlights Differences in Free Fatty Acid Composition between the Wild Type and Mutants

Finally, the solution NMR spectra of cutins purified by cholinium hexanoate and the matching cuticles (both of which were solubilized in DMSO-d_6 with the aid of cryogenic milling) strengthened the observation that some free hydroxyls exist in situ, consistent with previous reports (Petit et al., 2016; Philippe et al., 2016). Results from a systematic NMR analysis of cutins purified by cholinium hexanoate, from both wild type and mutants of the same cultivar (cv Micro-Tom), show increased diversity of fatty acids in both mutants, yet only the *cus1* mutant shows a substantially reduced esterification degree. These results are consistent with the functions of the enzymes inactivated in the mutants: *CUS1* is a polymerizing enzyme (Girard et al., 2012; Yeats et al., 2012), while *GPAT6* catalyzes the synthesis of cutin precursors (Petit et al., 2016). Remarkably, these results are also consistent with already published information on the mutants, obtained through a totally independent approach (Philippe et al., 2016). In situ analysis of cutin esterification levels by benzyl etherification of enzyme-treated cutin from tomato fruit peel showed that all/midchain hydroxylation of dihydroxy acids is increased strongly in the *cus1* mutant (linear polymers) but remains unaffected in the *gpat6* mutant, as in the wild type (normal interbranching).

Remarkably, the NMR results of the ionic liquid extracted cutins strongly suggest that naturally occurring free acids exist in the wild-type tomatoes (detected also in the cuticle) but are lacking in the mutants (and in their cuticles, as observed for the *cus1* cuticle). This might be due to the thinner mutant cuticles, where total esterification of the cutin monomers could be more easily achieved. This deserves a detailed analysis in the near future, especially as (1) we could not yet detect the signal assigned to β(C=O) acid, only that of the α(C=O) acids that was assigned through the HMBC spectrum; and (2) the signal assigned to the α(C=O) esters partially overlaps with that of the α(C=O) sugars in the analyzed tomato cutins.

CONCLUSIONS

The proof of concept of the efficiency and reliability of the ionic liquid cutin extraction method described here was established using tomato peel as a model. Because of its simplicity, this method should be broadly applicable to other tissues and to other plant model and crop species, as confirmed by preliminary experiments. In the near future quantitative methods (and better spectral resolution for solving yet unknown signals) will require development to understand better how cutin molecular structure (and its association with cuticular polysaccharides) is impacted by mutations or along the development of the plant. In addition, our study emphasizes the suitability of exploiting ionic liquid extraction as an easy and scalable approach for exploiting plant lipid polymers as a bioresource for a range of applications. The ionic liquid processes tested here can be systematically tuned (e.g. time, temperature, and component ions) to ensure recovery of cutin with different degrees of structural preservation. Finally, the solution NMR methodologies developed here constitute essential tools to fingerprint the multifunctionality and structure of cutin in planta. Based on all the analyses done on the polymer morphology, thermal properties, and chemistry, we are confident that short-time reactions with cholinium hexanoate can ensure the isolation of cutin with minimal disruption of its polymeric network, yielding the biopolymer in a near-native configuration.

MATERIALS AND METHODS

Plant Materials

Peels from the processing tomato (*Solanum lycopersicum* 'Roma') were manually removed, thoroughly washed, and then dried to a constant weight at 60°C. After drying, the peels were milled using a Retsch ZM200 electric grinder (granulometry 0.5 mm; 10,000 rpm) and stored at room temperature for further processing. 'Micro-Tom' tomatoes from both wild-type plants and mutant plants generated by ethyl methanesulfonate mutagenesis (Just et al., 2013) were cultivated as previously reported (Rothan et al., 2016) and processed as described above. All tomato fruits used were in the red ripe developmental stage.

Chemicals

BMIM acetate (>98%) was purchased from IoLiTec. Sodium hydroxide (>98%) was from José Manuel Gomes dos Santos. Methanol (≥99.8%), DMSO (>99.99%), hexane (>95%), chloroform (>99.98%), and dichloromethane (>99.99%) were from Fisher Chemical. Cholinium hydrogen carbonate (~80% in water), hexanoic acid (>99.5%), sodium azide (≥99.5%), sodium acetate (≥99%), cellulase (*Aspergillus niger*), and pectinase (*Aspergillus aculeatus*) were from Sigma Aldrich. Cholinium hexanoate was synthesized by dropwise addition of hexanoic acid to aqueous cholinium hydrogen carbonate in equimolar quantities, as previously described (Petkovic et al., 2010).

Ionic Liquid Hydrolysis of Standard Fatty Acids

Glyceryl trioctanoate and octyl octanoate (~50 mg) were mixed with either ionic liquid (1:10) at 100°C, without stirring, for 2, 6, or 24 h. At the end of the reaction, the mixture was rapidly cooled to room temperature in ice, acidified to pH 3/3.5 with 1 M HCl solution, spiked with a known concentration of heptadecanoic acid (internal standard), and extracted three times using dichloromethane/water partition. The dried combined organic phases were derivatized with N,O-bis(trimethylsilyl)trifluorocetamide in pyridine (5:1) for 30 min at 90°C. The TMS derivatives in the organic fractions were then analyzed by GC-MS as previously described (Ferreira et al., 2014), with minor modifications (ramp temperature 60°C; 4°C/min to 280°C for 15 min, with source at 230°C

and electron impact ionization of 70 eV; see equipment in the "GC-MS Data" section). Triplicate independent reactions were performed.

Cutin Extractions

Enzymatic Process

Cutin was isolated from tomato as previously described (Chatterjee et al., 2012). In brief, tomato peels were immersed in an enzymatic cocktail containing 4 mL pectinase, 0.2 g cellulase, 13 mg NaN_3, and 196 mL of 50 mM sodium acetate buffer and incubated at 31°C for 24 h with constant shaking. The isolated cuticles were successively dewaxed for 36 h by Soxhlet extraction with methanol, chloroform, and hexane (1:1:1), finally freeze dried, and stored at room temperature. This cutin enriched material was used as a reference material for the optimization phase of this study, i.e. selection of a suitable ionic liquid process.

Ionic Liquid Process

Cutin was extracted from tomato peels as previously described for suberin from cork (Ferreira et al., 2014), with slight modifications. In brief, 2 g of tomato peel powder were mixed in 20 g cholinium hexanoate or BMIM acetate and incubated for a defined period of time at 100°C, without stirring. The reaction was stopped by the addition of 160 mL DMSO. The polymer was recovered by filtration using a nylon membrane filter (0.45 μm); then washed with an excess of deionized water with the aid of centrifugation (Eppendorf 5804 R centrifuge, 5,000 rpm at 4°C for 30 min).

Treatment of Cutin Extracted Using Cholinium Hexanoate (2 h) with TFA

Six hundred milligrams of the cutin-enriched material obtained through extraction with cholinium hexanoate for 2 h was treated with 1 M of aqueous TFA solution for 60 min at 110°C. The reaction mixture was filtered, and the insoluble material was washed with stirring using chloroform-methanol (1:1 [v/v]) for 2 h. The organic-insoluble material was separated by filtration, freeze-dried, and analyzed by ^{13}C MAS NMR.

Microscopic Analyses

SEM (JSM-7001F, JEOL) was used to analyze the cutin-enriched materials.

Cryogenic Grinding Process

A RESTCH Cryomill equipped with a 25 mL grinding jar with six zirconium oxide grinding balls (10 mm) was used. To optimize the solubilization level of the cutin-enriched materials needed to attain high NMR spectral resolution, cutin samples were cryogenically milled at −196°C (liquid nitrogen) as follows: 3 min of precooling followed by 9 milling cycles, each comprising 3 min of milling at 30 Hz plus 0.5 min of intermediate cooling at 5 Hz. The ensuing samples were analyzed by ^1H NMR (3 mg dissolved in 400 μL of DMSO-d_6) and the 200 milling cycles were selected to systematically process cutin samples before 2D NMR analysis.

NMR Analysis

^{13}C MAS NMR spectra were acquired on the cutin-enriched materials (±250 mg), which were packed into 7 mm o.d. zirconia rotors (after grinding if needed), equipped with Kel-F caps. ^{13}C MAS with high-power continuous-wave decoupling spectra were obtained at 75.49 MHz, on a Tecmag Redstone/Bruker 300WB, with spinning rates of 3.1 to 3.3 kHz. In these experiments, 90° radio frequency pulses of ~4.5 μs and relaxation delays of 3 s were used. ^{13}C chemical shifts were referenced with respect to external Gly (^{13}CO observed at 176.03 ppm).

Solution-state NMR spectra of the cutin samples solubilized with the aid of cryogenic milling (see the "Cryogenic Grinding Process" section) were recorded using an Avance II + 800 MHz spectrometer (Bruker Biospin), with the exception of ^1H-^{13}C HMBC spectra, which were acquired using an Avance III 800 CRYO (Bruker Biospin). All NMR spectra (^1H, ^1H-^1H COSY, and ^1H-^{13}C HSQC) were acquired using 5-mm-diameter NMR tubes at 60°C with 3 mg of cryomilled cutin in 400 μL DMSO-d_6.

MestReNova version 11.04-18998 (Mestrelab Research) was used to process the raw data acquired in the Bruker spectrometers.

DSC Data

Calorimetric analyses of the cutin-enriched materials were carried out in a TA Instruments Q200 calorimeter connected to a cooling system and calibrated with different standards (indium and empty cap). Sample weights ranged from 9 to 11 mg. A temperature interval from −80°C to 220°C was studied and the heating/cooling rate was 10°C min^{-1}.

WAXS Data

WAXS data of the cutin-enriched materials were collected using a laboratory SAXS/WAXS beamline (Xeuss 2.0, Xenocs) equipped with a liquid gallium MetalJet x-ray source (Excillum; wavelength λ = 1.34 Å), FOX 3D Ga single-reflection x-ray mirror and two sets of motorized scatterless slits for beam collimation, and a Pilatus 100k 2D pixel WAXS detector (Dectris). Loose cutin powder samples were enclosed between two flat kapton films and mounted on the beamline sample stage (the total sample thickness is ~1 mm). 2D WAXS patterns were recorded in a transmission mode over a q range of 1.3 $Å^{-1}$ to 3.5 $Å^{-1}$ [where $q = (4\pi\sin\theta)/\lambda = 2\pi/d$ is the length of the scattering vector, θ is one-half of the scattering angle, and d is the spacing in real space] using an exposure time of 1,200 s. The WAXS data were reduced (calibrated, integrated, and background-subtracted) using the Foxtrot software package supplied with the instrument.

GC-MS Data

A gas chromatograph (7820A, Agilent) equipped with a mass spectrometer (5977B, Agilent; quadrupole) was used. First, to release the hydrolyzable constituents, the cutin-enriched materials were treated with a solution of 0.5 M NaOH in methanol:water (1:1 [v/v]) at 95°C for 4 h, cooled to room temperature, and acidified to pH 3/3.5 with 1 M HCl, then extracted by dichloromethane/water partition (5×). The nonhydrolyzable fraction was recovered by filtration (0.2-μm nylon filters), washed, freeze-dried, and weighted (recalcitrance). The dried combined organic extracts were sequentially derivatized (30 min at 90°C): first, 2.0 M (trimethylsilyl)diazomethane in hexane, mixed in a methanol:toluene 2.5:1 solution (3:2); and second, N,O-bis(trimethylsilyl)trifluoroacetamide containing 1% (v/v) trimethylchlorosilane in pyridine (5:1). The derivatives were then analyzed by GC-MS (HP-5MS column) as follows: ramp temperature 80°C, then 4°C min^{-1} to 310°C for 15 min. The MS scan mode, with source at 230°C and electron impact ionization (EI+, 70 eV) was used for all samples. The GC-MS was first calibrated with pure reference compounds (representative monomers: heptadecanoic acid, hexadecanedioic acid, and ferulic acid) relative to hexadecane (internal standard). Each sample was analyzed in triplicate. Data acquisition was accomplished by MSD ChemStation (Agilent Technologies); compounds were identified based on the equipment spectral library (Wiley-National Institute of Standards and Technology) and references relying on diagnostic ions distinctive of each derivative and its spectrum profile (Supplemental Table S1).

Accession Numbers

Sequence data from this article can be found in the GenBank/EMBL data libraries under accession numbers Solyc11g006250 (CUS1) and Solyc09g014350 (GPATt6).

Supplemental Data

The following supplemental materials are available.

Supplemental Figure S1. ATR-FTIR of the soluble and insoluble fractions attained after the reaction of tomato peels with cholinium hexanoate (2 h at 100°C) compared to a cutin reference isolated using the conventional enzymatic hydrolysis.

Supplemental Figure S2. ^{13}C MAS NMR spectrum of the cutin extracted with cholinium hexanoate followed or not by acidic hydrolysis with

TFA. The signal previously assigned to the cholinium cation (54 ppm) was washed out.

Supplemental Figure S3. Representative cutin GC-MS chromatogram.

Supplemental Figure S4. 2D-^{1}H-^{1}H COSY-NMR spectrum of cutin extracted using cholinium hexanoate (2 h) in DMSO-d_6 at 60°C.

Supplemental Figure S5. 2D-^{1}H-^{13}C HSQC-NMR spectrum of cutin extracted using cholinium hexanoate (2 h) in DMSO-d_6 at 60°C.

Supplemental Figure S6. 2D-^{1}H-^{13}C HMBC-NMR spectrum of cutin extracted using cholinium hexanoate (2 h) in DMSO- d_6 at 60°C.

Supplemental Figure S7. 2D-^{1}H-^{13}C HSQC-NMR spectrum of cutin extracted using BMIM acetate (2 h) in DMSO-d_6 at 60°C, with the HSQC region corresponding to aliphatics magnified.

Supplemental Figure S8. 2D-^{1}H-^{1}H COSY-NMR spectrum of cv Micro-Tom cutin isolated with cholinium hexanoate (2 h) in DMSO-d_6 at 60°C.

Supplemental Figure S9. 2D-^{1}H-^{13}C HSQC-NMR spectrum of cv Micro-Tom cutin isolated with cholinium hexanoate (2 h) in DMSO-d_6 at 60°C.

Supplemental Figure S10. 2D-^{1}H-^{13}C HMBC-NMR spectrum of cv Micro-Tom cutin isolated with cholinium hexanoate (2 h) in DMSO-d_6 at 60°C.

Supplemental Figure S11. 2D-^{1}H-^{1}H COSY-NMR spectrum of cv Micro-Tom cuticle in DMSO-d_6 at 60°C.

Supplemental Figure S12. 2D-^{1}H-^{13}C HSQC-NMR spectrum of cv Micro-Tom cuticle in DMSO-d_6 at 60°C.

Supplemental Figure S13. Wide-ranging NMR spectral characterization of cv Micro-Tom from *cus1* untreated cuticle.

Supplemental Figure S14. 2D-^{1}H-^{1}H COSY-NMR spectrum of cv Micro-Tom cutin isolated with cholinium hexanoate (2 h) from the *cus1* mutant in DMSO-d_6 at 60°C.

Supplemental Figure S15. 2D-^{1}H-^{13}C HSQC-NMR spectrum of cv Micro-Tom cutin isolated with cholinium hexanoate (2 h) from the *cus1* mutant in DMSO-d_6 at 60°C.

Supplemental Figure S16. 2D-^{1}H-^{13}C HMBC-NMR spectrum of cv Micro-Tom cutin isolated with cholinium hexanoate (2 h) from the *cus1* mutant in DMSO-d_6 at 60°C.

Supplemental Figure S17. 2D-^{1}H-^{1}H COSY-NMR spectrum of cv Micro-Tom cutin isolated with cholinium hexanoate (2 h) from the *gpat6* mutant in DMSO-d_6 at 60°C.

Supplemental Figure S18. 2D-^{1}H-^{13}C HSQC-NMR spectrum of cv Micro-Tom cutin isolated with cholinium hexanoate (2 h) from the *gpat6* mutant in DMSO-d_6 at 60°C.

Supplemental Figure S19. 2D-^{1}H-^{13}C HMBC-NMR spectrum of cv Micro-Tom cutin isolated with cholinium hexanoate (2 h) from the *gpat6* mutant in DMSO-d_6 at 60°C.

Supplemental Figure S20. Overlaps of the 2D-^{1}H-^{13}C HSQC-NMR spectra of cv Micro-Tom cutins isolated with cholinium hexanoate (2 h) from the wild type (gray) and the *cus1* (red) and *gpat6* (blue) mutants in DMSO-d_6 at 60°C.

Supplemental Table S1. Diagnostic ions used to identify the monomers extracted from tomato cutin and their retention times (Rt).

Supplemental Table S2. Elemental analysis of cutin purified after treatment with cholinium hexanoate for 2 h before and after cryogenic milling.

Supplemental Table S3. Monomeric composition of cutin extracted using cholinium hexanoate (2 h), as identified by NMR, showing chemical structures and ^{1}H and ^{13}C chemical shifts (ppm) of the cutin monomers.

ACKNOWLEDGMENTS

The authors are grateful to Manolis Matzapetakis (Instituto de Tecnologia Química e Biológica António Xavier, Universidade Nova de Lisboa [ITQB NOVA]) and Maria João Ferreira (Instituto Superior Tecnico) for support in the solid-state NMR analyses and to Pedro Lamosa and Maria C. Leitão (ITQB NOVA) for support in the solution NMR and chromatographic analyses, respectively. The solution NMR data were acquired at the ITQB-NOVA with equipment funded by the Fundação para a Ciência e a Tecnologia. Finally, we are extremely grateful to Bénédicte Bakan and Didier Marion for fruitful scientific discussions during the manuscript preparation.

Received August 3, 2020; accepted August 3, 2020; published August 11, 2020.

LITERATURE CITED

Arrieta-Baez D, Stark RE (2006) Using trifluoroacetic acid to augment studies of potato suberin molecular structure. J Agric Food Chem **54:** 9636–9641

Bakan B, Marion D (2017) Assembly of the cutin polyester: From cells to extracellular cell walls. Plants (Basel) **6:** 57

Benítez JJ, Castillo PM, Del Río JC, León-Camacho M, Domínguez E, Heredia A, Guzmán-Puyol S, Athanassiou A, Heredia-Guerrero JA (2018) Valorization of tomato processing by-products: Fatty acid extraction and production of bio-based materials. Materials (Basel) **11:** 2211

Bunn CW (1944) The crystal structure of ethylene. Trans Faraday Soc **40:** 23–25

Chassot C, Nawrath C, Métraux JP (2007) Cuticular defects lead to full immunity to a major plant pathogen. Plant J **49:** 972–980

Chatterjee S, Matas AJ, Isaacson T, Kehlet C, Rose JKC, Stark RE (2016) Solid-state ^{13}C NMR delineates the architectural design of biopolymers in native and genetically altered tomato fruit cuticles. Biomacromolecules **17:** 215–224

Chatterjee S, Sarkar S, Oktawiec J, Mao Z, Niitsoo O, Stark RE (2012) Isolation and biophysical study of fruit cuticles. J Vis Exp **2012:** 3529

Correia VG, Bento A, Pais J, Rodrigues R, Halińsk ŁP, Frydrych M, Greenhalgh A, Stepnowski P, Vollrath F, King AWT, et al (2020) The molecular structure and multi-functionality of the cryptic plant polymer suberin. Mater Today Bio **5:** 10039

Deshmukh AP, Simpson AJ, Hatcher PG (2003) Evidence for cross-linking in tomato cutin using HR-MAS NMR spectroscopy. Phytochemistry **64:** 1163–1170

España L, Heredia-Guerrero JA, Segado P, Benítez JJ, Heredia A, Domínguez E (2014) Biomechanical properties of the tomato (*Solanum lycopersicum*) fruit cuticle during development are modulated by changes in the relative amounts of its components. New Phytol **202:** 790–802

Fawke S, Torode TA, Gogleva A, Fich EA, Sørensen I, Yunusov T, Rose JKC, Schornack S (2019) Glycerol-3-phosphate acyltransferase 6 controls filamentous pathogen interactions and cell wall properties of the tomato and *Nicotiana benthamiana* leaf epidermis. New Phytol **223:** 1547–1559

Fernández V, Guzmán-Delgado P, Graça J, Santos S, Gil L (2016) Cuticle structure in relation to chemical composition: Re-assessing the prevailing model. Front Plant Sci **7:** 427

Ferreira R, Garcia H, Sousa AF, Guerreiro M, Duarte FJS, Freire CSR, Calhorda MJ, Silvestre AJD, Kunz W, Rebelo LPN, et al (2014) Unveiling the dual role of the cholinium hexanoate ionic liquid as solvent and catalyst in suberin depolymerisation. RSC Advances **4:** 2993–3002

Ferreira R, Garcia H, Sousa AF, Petkovic M, Lamosa P, Freire CSR, Silvestre AJD, Rebelo LPN, Silva Pereira C (2012) Suberin isolation from cork using ionic liquids: Characterisation of ensuing products. New J Chem **36:** 2014–2024

Fich EA, Segerson NA, Rose JKC (2016) The plant polyester cutin: Biosynthesis, structure, and biological roles. Annu Rev Plant Biol **67:** 207–233

Garcia H, Ferreira R, Petkovic M, Ferguson JL, Leitão MC, Gunaratne HQN, Seddon KR, Rebelo LPN, Silva Pereira C (2010) Dissolution of cork biopolymers in biocompatible ionic liquids. Green Chem **12:** 367–369

Garcia V, Bres C, Just D, Fernandez L, Tai FWJ, Mauxion JP, Le Paslier MC, Bérard A, Brunel D, Aoki K, et al (2016) Rapid identification of causal mutations in tomato EMS populations via mapping-by-sequencing. Nat Protoc **11:** 2401–2418

Girard AL, Mounet F, Lemaire-Chamley M, Gaillard C, Elmorjani K, Vivancos J, Runavot JL, Quemener B, Petit J, Germain V, et al (2012) Tomato GDSL1 is required for cutin deposition in the fruit cuticle. Plant Cell **24:** 3119–3134

Graça J, Lamosa P (2010) Linear and branched poly(ω-hydroxyacid) esters in plant cutins. J Agric Food Chem **58:** 9666–9674

Heredia-Guerrero JA, Heredia A, Domínguez E, Cingolani R, Bayer IS, Athanassiou A, Benítez JJ (2017) Cutin from agro-waste as a raw material for the production of bioplastics. J Exp Bot **68:** 5401–5410

Hernández Velasco BL, Arrieta-Baez D, Cortez Sotelo PI, Méndez-Méndez JV, Berdeja Martínez BM, Gómez-Patiño MB (2017) Comparative studies of cutins from lime (*Citrus aurantifolia*) and grapefruit (*Citrus paradisi*) after TFA hydrolysis. Phytochemistry **144:** 78–86

Ingram G, Nawrath C (2017) The roles of the cuticle in plant development: Organ adhesions and beyond. J Exp Bot **68:** 5307–5321

Just D, Garcia V, Fernandez L, Bres C, Mauxion J-P, Petit J, Jorly J, Assali J, Bournonville C, Ferrand C, et al (2013) Micro-Tom mutants for functional analysis of target genes and discovery of new alleles in tomato. Plant Biotechnol (Tokyo) **30:** 225–231

Li Y, Wang J, Liu X, Zhang S (2018) Towards a molecular understanding of cellulose dissolution in ionic liquids: Anion/cation effect, synergistic mechanism and physicochemical aspects. Chem Sci (Camb) **9:** 4027–4043

Lyerla JR (1980) High-resolution nuclear magnetic resonance spectroscopy. *In* RA Fava, ed, Polymers: Molecular Structure and Dynamics, Methods in Experimental Physics, Vol 16A, Elsevier, Amsterdam, pp 241–369

Matas AJ, Yeats TH, Buda GJ, Zheng Y, Chatterjee S, Tohge T, Ponnala L, Adato A, Aharoni A, Stark R, et al (2011) Tissue- and cell-type specific transcriptome profiling of expanding tomato fruit provides insights into metabolic and regulatory specialization and cuticle formation. Plant Cell **23:** 3893–3910

Mazurek S, Garroum I, Daraspe J, De Bellis D, Olsson V, Mucciolo A, Butenko MA, Humbel BM, Nawrath C (2017) Connecting the molecular structure of cutin to ultrastructure and physical properties of the cuticle in petals of Arabidopsis. Plant Physiol **173:** 1146–1163

Mykhaylyk OO, Smith KW, Martin CM, Ryan AJ (2007) Structural models of metastable phases occurring during the crystallization process of saturated/unsaturated triacylglycerols. J Appl Crystallogr **40:** s297–s302

Nawrath C, Schreiber L, Franke RB, Geldner N, Reina-Pinto JJ, Kunst L (2013) Apoplastic diffusion barriers in Arabidopsis. The Arabidopsis Book **11:** e0167 doi:10.1199/tab.0167

Petit J, Bres C, Mauxion J-P, Bakan B, Rothan C (2017) Breeding for cuticle-associated traits in crop species: traits, targets, and strategies. J Exp Bot **68:** 5369–5387

Petit J, Bres C, Mauxion JP, Tai FWJ, Martin LBB, Fich EA, Joubès J, Rose JKC, Domergue F, Rothan C (2016) The glycerol-3-phosphate acyltransferase GPAT6 from tomato plays a central role in fruit cutin biosynthesis. Plant Physiol **171:** 894–913

Petkovic M, Ferguson JL, Gunaratne HQN, Ferreira R, Leitão MC, Seddon KR, Rebelo LPN, Silva Pereira C (2010) Novel biocompatible cholinium-based ionic liquids—Toxicity and biodegradability. Green Chem **12:** 643–649

Philippe G, Gaillard C, Petit J, Geneix N, Dalgalarrondo M, Bres C, Mauxion J-P, Franke R, Rothan C, Schreiber L, et al (2016) Ester cross-link profiling of the cutin polymer of wild-type and cutin synthase tomato mutants highlights different mechanisms of polymerization. Plant Physiol **170:** 807–820

Philippe G, Geneix N, Petit J, Guillon F, Sandt C, Rothan C, Lahaye M, Marion D, Bakan B (2020) Assembly of tomato fruit cuticles: A cross-talk between the cutin polyester and cell wall polysaccharides. New Phytol **226:** 809–822

Rogers RD, Seddon KR (2003) Chemistry. Ionic liquids—solvents of the future? Science **302:** 792–793

Rongpipi S, Ye D, Gomez ED, Gomez EW (2019) Progress and opportunities in the characterization of cellulose—an important regulator of cell wall growth and mechanics. Front Plant Sci **9:** 1894

Rothan C, Just D, Fernandez L, Atienza I, Ballias P, Lemaire-Chamley M (2016) Culture of the tomato Micro-Tom cultivar in greenhouse. *In* JR Botella, MA Botella, eds, Plant Signal Transduction: Methods and Protocols, Methods in Molecular Biology, Vol 1363. Humana Press, Totowa, NJ, pp 57–64

Segado P, Domínguez E, Heredia A (2016) Ultrastructure of the epidermal cell wall and cuticle of tomato fruit (*Solanum lycopersicum* L.) during development. Plant Physiol **170:** 935–946

Small DM (1984) Lateral chain packing in lipids and membranes. J Lipid Res **25:** 1490–1500

Southern JH, Weeks N, Porter RS, Crystal RG (1972) Unique polyethylene morphologies produced under extrusion conditions. Macromol Chem Phys **162:** 19–30

Yeats TH, Huang W, Chatterjee S, Viart HMF, Clausen MH, Stark RE, Rose JKC (2014) Tomato Cutin Deficient 1 (CD1) and putative orthologs comprise an ancient family of cutin synthase-like (CUS) proteins that are conserved among land plants. Plant J **77:** 667–675

Yeats TH, Martin LBB, Viart HMF, Isaacson T, He Y, Zhao L, Matas AJ, Buda GJ, Domozych DS, Clausen MH, et al (2012) The identification of cutin synthase: Formation of the plant polyester cutin. Nat Chem Biol **8:** 609–611

Zhang X, Zhang A, Liu C, Ren J (2016) Per-O-acylation of xylan at room temperature in dimethylsulfoxide/N-methylimidazole. Cellulose **23:** 2863–2876